Applied Catalysis B: Environmental 183 (2016) 426–432

Contents lists available at ScienceDirect

Applied Catalysis B: Environmental

journal homepage: www.elsevier.com/locate/apcatb

Facile synthesis and enhanced visible-light photoactivity of $DyVO_4/g\text{-}C_3N_4I$ composite semiconductors

Huiquan Li[a,b], Yuxing Liu[a], Yumin Cui[b], Wenbao Zhang[b], Cong Fu[b], Xinchen Wang[a,*,1]

[a] State Key Laboratory of Photocatalysis on Energy and Environment, College of Chemistry, Fuzhou University, Fuzhou 350002, PR China
[b] School of Chemistry and Materials Engineering, Fuyang Normal College, Fuyang 236037, PR China

ARTICLE INFO

Article history:
Received 11 October 2015
Received in revised form
11 November 2015
Accepted 14 November 2015
Available online 18 November 2015

Keywords:
$DyVO_4$
$g\text{-}C_3N_4I$
Conjugated polymer
Visible-light photocatalysis

ABSTRACT

$DyVO_4$/iodine modified graphitic carbon nitride ($DyVO_4/g\text{-}C_3N_4I$) composite semiconductors with different weight percents of $DyVO_4$ were successfully synthesized by a facile heating method, and characterized by X-ray diffraction (XRD), X-ray photoelectron spectroscopy (XPS), transmission electron microscopy (TEM), UV–vis diffuse reflection spectroscopy (UV–vis DRS), photoluminescence (PL) and electron paramagnetic resonance (EPR) spectra, N_2 adsorption–desorption analysis and photo-electrochemical measurement. The resulting $DyVO_4/g\text{-}C_3N_4I$ semiconductor with a suitable weight percents of 6.3% $DyVO_4$ showed the highest visible-light photoactivity, and its degradation ratio for methylene blue was more than 1.8 time higher than that of $DyVO_4$, $g\text{-}C_3N_4$ and $g\text{-}C_3N_4I$. The H_2 evolution rate of 6.3% $DyVO_4/g\text{-}C_3N_4I$ was 10.6, 4.7 and 1.7 times higher than that of $DyVO_4$, $g\text{-}C_3N_4$ and $g\text{-}C_3N_4I$, respectively, while still having excellent reusability and stability. The obviously enhanced photoactivity of 6.3% $DyVO_4/g\text{-}C_3N_4I$ is mainly ascribed to the fact that the proper $DyVO_4$ modified $g\text{-}C_3N_4I$ increase its specific surface area, decrease band-gap energy, enhance absorption in the 400–700 nm region and promote efficient separation of photo-generated carriers. The mechanism on the improvement of visible-light photoactivity is discussed.

1. Introduction

Polymeric graphitic carbon nitride ($g\text{-}C_3N_4$) photocatalyst possesses many fascinating properties, such as metal-free semiconductor, environmentally benign, good thermal and chemical stability, appropriate conduction band and valence band positions [1–7]. Over the past several years, $g\text{-}C_3N_4$ photocatalyst attracted great attention owing to its successful application in photocatalytic hydrogen evolution [1,8], CO_2 reduction [9] and contaminant removal [10,11] under visible light irradiation, while the photocatalytic activity of pristine $g\text{-}C_3N_4$ is moderate. Recently, it has been found that iodine modified graphitic carbon nitride ($g\text{-}C_3N_4I$) semiconductors possess large charge carrier mobility, strong visible-light harvesting and obvious changes of energy band structure, compared with pristine $g\text{-}C_3N_4$ [12,13]. Nowadays, $g\text{-}C_3N_4I$ photocatalyst has become a research hot topic in the field of environmental and energy science [12], which calls for the further modification and development of $g\text{-}C_3N_4I$ for solar photocatalysis applications.

Previous studies have shown that the construction of $g\text{-}C_3N_4$-based composite materials can enhance the separation efficiency of photo-induced carriers at the heterojunction of composites to improve photocatalytic properties [4–7,11,14–18]. For example, Dontsova et al. [19] developed a SnO_2/carbon nitride composite photocatalyst to improve the hydrogen evolution of mesoporous carbon nitride under visible light irradiation, and Yan et al. [20] prepared N-doped ZnO/$g\text{-}C_3N_4$ core–shell nanoplate with higher visible-light activity than either a single phase of $g\text{-}C_3N_4$ or N-doped ZnO for the degradation of Rhodamine B.

$DyVO_4$ has a small band gap (~2.3 eV) and shows a strong absorption in the visible-light region [21]. Moreover, $DyVO_4$ has a matching conduction band and valence band position with $g\text{-}C_3N_4I$ [12,13,21]. In theory, the coupling of $DyVO_4$ with $g\text{-}C_3N_4I$ can allow band alignment to promote the separation of photo-generated electron–hole pairs. Therefore, the $DyVO_4/g\text{-}C_3N_4I$ composite may be a hopeful candidate of efficient photocatalysts.

In this work, $DyVO_4/g\text{-}C_3N_4I$ composite photocatalysts with different weight percents of $DyVO_4$ were successfully synthesized by a facile heating method at 550 °C for 4.0 h, and the effect of $DyVO_4$ contents on the structure and photocatalytic activity of

* Corresponding author. Fax: +86 591 83920097.
E-mail address: xcwang@fzu.edu.cn (X. Wang).
[1] http://wanglab.fzu.edu.cn.

http://dx.doi.org/10.1016/j.apcatb.2015.11.012
0926-3373/

$DyVO_4$/g-C_3N_4I catalysts was studied in details. The structure of $DyVO_4$/g-C_3N_4I catalysts was characterized by XRD, XPS, TEM, PL, EPR, UV–vis DRS, N_2 adsorption–desorption analysis and photoelectrochemical measurements. The visible-light photoactivity of $DyVO_4$/g-C_3N_4I for H_2 evolution and methylene blue degradation was greatly enhanced as compared to either g-C_3N_4I or $DyVO_4$. The transfer process of photo-induced carriers was proposed based on the band structures of $DyVO_4$ and g-C_3N_4I. This work describes a visible-light responsive $DyVO_4$/g-C_3N_4I composite semiconductor with potential in energy and environmental applications.

2. Experimental

2.1. Synthesis of photocatalysts

The synthetic procedure of $DyVO_4$ was as follows: $Dy(NO_3)_3$ and NH_4VO_3 were separately dissolved in deionized water in a same molar ratio. Then, the two solutions were mixed to produce a yellow precipitate. The pH value of above solutions was adjusted to 7.0 by a solution of NH_3. After being aged for 4.0 h at room temperature, the deposit was filtered and washed several times with deionized water, dried at 110 °C for 10 h, and calcined at 500 °C for 2.0 h using air atmosphere.

The $DyVO_4$/g-C_3N_4I composites were synthesized by a heating method. Firstly, the iodine doped g-C_3N_4I catalyst was prepared by mixing dicyandiamide (2.0 g) with ammonium iodine (1.0 g) in 15 mL deionized water under stirring at 80 °C to remove water, and then the resultant solids were mixed with a certain of $DyVO_4$ and ground in an agate mortar for 30 min. Secondly, the mixture was calcined at 550 °C for 4.0 h at air atmosphere. The weight percents of $DyVO_4$ in the $DyVO_4$/g-C_3N_4I composites were obtained by energy dispersive analysis of X-rays (EDX), and were denoted as 3.2%, 6.3%, and 9.7% $DyVO_4$/g-C_3N_4I, respectively. For comparison purpose, g-C_3N_4I catalyst was prepared by a similar method at the absence of $DyVO_4$, and the pristine g-C_3N_4 catalyst was synthesized by a derectly calcination of dicyandiamide at 550 °C for 4 h at air.

2.2. Characterization

The XRD measurements of samples were performed at a BrukerD8 X-ray diffractometer using Cu Kα radiation (λ = 0.15418 nm). Transmission electron microscope (TEM) images of samples were collected from JEM-200CX. X-ray photo-electron spectroscopy (XPS) measurements of samples were carried out on a PHI 5000 VersaProbe instrument. The UV–vis diffuse reflectance spectra (UV–vis DRS) were recorded by a spectrophotometer (TU-1901). The photoluminescence (PL) spectra of as-fabricated samples were collected by FluoroMax-4 (HORIBA, USA) with an excitation wavelength at 400 nm. Specific surface areas and pore structures of the samples were recorded from N_2 adsorption–desorption isotherms at 77 K, using an ASAP2020HD88 instrument. EPR spectra were determined by using a Bruker model A300 spectrometer. Photoelectrochemical measurements were performed by a BAS Epsilon Electrochemical System under visible-light irradiation with a conventional three electrode cell, immersing in 50 mL solution of 0.1 M Na_2SO_4 (pH 6.8). The sample electrodes were used as the working electrodes, which were fabricated on indium-tin oxide (ITO) conductor glasses. Powder samples (10 mg) were dispersed in 800 μL *N*,*N*-dimethylformamide with sonication to get a slurry mixture. The slurry was spread onto ITO glass whose side part was previously protected through a Scotch tape. The working electrode was dried overnight at ambient conditions. Uncoated parts of the electrode were isolated with epoxy resin. Pt plate and Ag/AgCl (3 mol/L KCl) electrodes were used as a reference and a counter electrode, respectively. A 300 W Xe lamp was employed as the excitation light source, and combined with a visible light band-pass filter (greater than 420 nm).

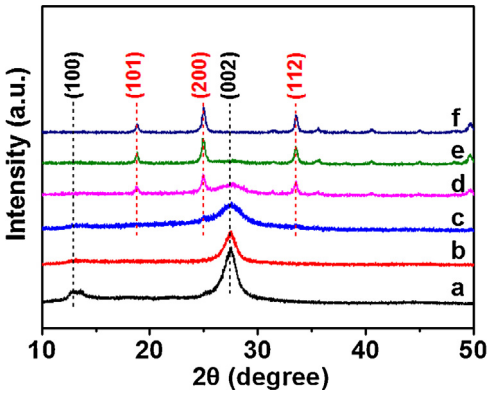

Fig. 1. XRD patterns of (a) g-C_3N_4, (b) g-C_3N_4I, (c) 3.2% $DyVO_4$/g-C_3N_4I, (d) 6.3% $DyVO_4$/g-C_3N_4I, (e) 9.7% $DyVO_4$/g-C_3N_4I, and (f) $DyVO_4$ samples.

2.3. Photocatalytic test

The photo-degradation of methylene blue for as-prepared samples was carried out in a photoreaction apparatus under a 500 W Xe lamp irradiation with a 420 nm cut-off filter. For photocatalytic reaction, 0.2 g of catalyst was put into 50 mL (10 mg/L) methylene blue solution. Prior to visible-light irradiation, the suspension was magnetically stirred for 1.0 h to reach an adsorption–desorption equilibrium in the dark. About 3.0 mL liquid was taken at given time interval of irradiation and centrifuged to remove the catalyst for analysis by a TU-1901 spectroscopy.

H_2 evolution was performed by the dispersion of catalyst (50 mg) in an 100 mL aqueous solution that contained triethanolamine (10 vol%), and 3 wt% Pt was loaded onto the surface of the catalyst by the in situ photo-deposition method using H_2PtCl_6 as starting material. The reactant solution was evacuated several times to remove air before visible-light irradiation, which was generated by using a 300 W Xe lamp attached to a 420 nm cut-off filter. During the reaction, the temperature of the reactant solution was maintained at room temperature by a flow of cooling water. The evolved gases were analyzed by a gas chromatography (Shimadzu, GC-8A).

3. Results and discussion

3.1. Characterization

Fig. 1 shows the XRD patterns of g-C_3N_4, g-C_3N_4I, 3.2% $DyVO_4$/g-C_3N_4I, 6.3% $DyVO_4$/g-C_3N_4I, 9.7% $DyVO_4$/g-C_3N_4I and $DyVO_4$ samples. One distinct peak is found in g-C_3N_4 and g-C_3N_4I at 27.4°, corresponding to the stacking of the CN-conjugated layers along the (0 0 2) direction [14,22]. $DyVO_4$ presents several robust diffraction peaks at 18.7°, 24.9° and 33.5°, which were indexed to those of tetragonal $DyVO_4$ and correspond to (1 0 1), (2 0 0), and (1 1 2) crystal plane [23], respectively. With the increase of $DyVO_4$ content in the $DyVO_4$/g-C_3N_4I composites, the $DyVO_4$ peaks gradually strengthen at the expense of those of g-C_3N_4I, which verify the co-existence of both $DyVO_4$ and g-C_3N_4I phases in $DyVO_4$/g-C_3N_4I hybrid materials.

Fig. 2 exhibits the X-ray photoelectron spectroscopy (XPS) of g-C_3N_4I and 6.3% $DyVO_4$/g-C_3N_4I samples. Obviously, the high resolution XPS spectra of I 3d indicates two peaks centered at 621.5 and 633.3 eV, corresponding to the I $3d_{5/2}$ and I $3d_{3/2}$ [12], respectively. This result confirms the existence of iodine in g-C_3N_4I and $DyVO_4$/g-C_3N_4I samples.

Table 1
Physicochemical properties of g-C_3N_4, g-C_3N_4I, $DyVO_4$ and $DyVO_4$/g-C_3N_4I samples.

Sample	Specific surface area (m^2/g)	Pore volume (cm^3/g)	Average pore size (nm)	Band gap (eV)
g-C_3N_4	7	0.02	8.5	2.70
g-C_3N_4I	22	0.06	9.9	2.68
3.2% $DyVO_4$/g-C_3N_4I	34	0.07	5.8	2.65
6.3% $DyVO_4$/g-C_3N_4I	50	0.10	8.0	2.61
9.7% $DyVO_4$/g-C_3N_4I	42	0.08	8.6	2.64
$DyVO_4$	20	0.05	10.4	2.32

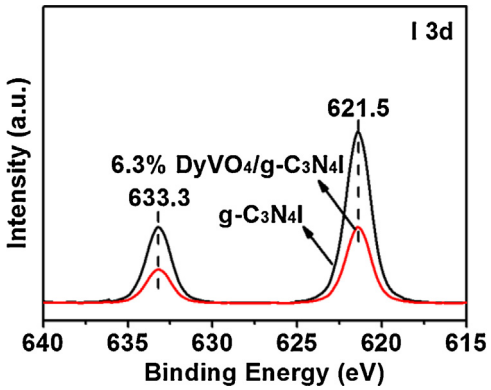

Fig. 2. XPS spectra of g-C_3N_4I and 6.3% $DyVO_4$/g-C_3N_4I samples.

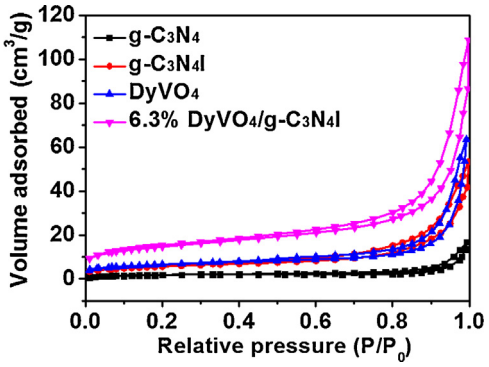

Fig. 3. Nitrogen adsorption–desorption isotherms of g-C_3N_4, g-C_3N_4I, $DyVO_4$ and 6.3% $DyVO_4$/g-C_3N_4I samples.

The N_2 adsorption–desorption isotherms of g-C_3N_4, g-C_3N_4I, $DyVO_4$ and 6.3% $DyVO_4$/g-C_3N_4I samples are indicated in Fig. 3. It can be observed that all of the isotherms are of type IV, usually associated with capillary condensation in mesopores [14,24,25]. The specific surface area, pore volume, and average pore size of g-C_3N_4, g-C_3N_4I, 3.2% $DyVO_4$/g-C_3N_4I, 6.3% $DyVO_4$/g-C_3N_4I, 9.7% $DyVO_4$/g-C_3N_4I and $DyVO_4$ samples are listed in Table 1.

The specific surface area of 6.3% $DyVO_4$/g-C_3N_4I is 50 m^2/g, which is higher than that of g-C_3N_4, g-C_3N_4I, 3.2% $DyVO_4$/g-C_3N_4I, 9.7% $DyVO_4$/g-C_3N_4I and $DyVO_4$ at 7, 22, 34, 42 and 20 m^2/g, respectively. The pore size of the samples is estimated by the Barrett–Joyner–Halenda (BJH) method, and the pore diameters of g-C_3N_4, g-C_3N_4I, 3.2% $DyVO_4$/g-C_3N_4I, 6.3% $DyVO_4$/g-C_3N_4I, 9.7% $DyVO_4$/g-C_3N_4I and $DyVO_4$ samples are approximately 8.5, 9.9, 5.8, 8.0, 8.6 and 10.4 nm, respectively. The pore volume of 6.3% $DyVO_4$/g-C_3N_4I is 0.10 cm^3/g, which is larger than that of g-C_3N_4, g-C_3N_4I, 3.2% $DyVO_4$/g-C_3N_4I, 9.7% $DyVO_4$/g-C_3N_4I and $DyVO_4$ at 0.02, 0.06, 0.07, 0.08 and 0.05 cm^3/g, respectively. The higher specific surface area and pore volume of the 6.3% $DyVO_4$/g-C_3N_4I sample are likely to contribute to the enhancement of the photoactivity.

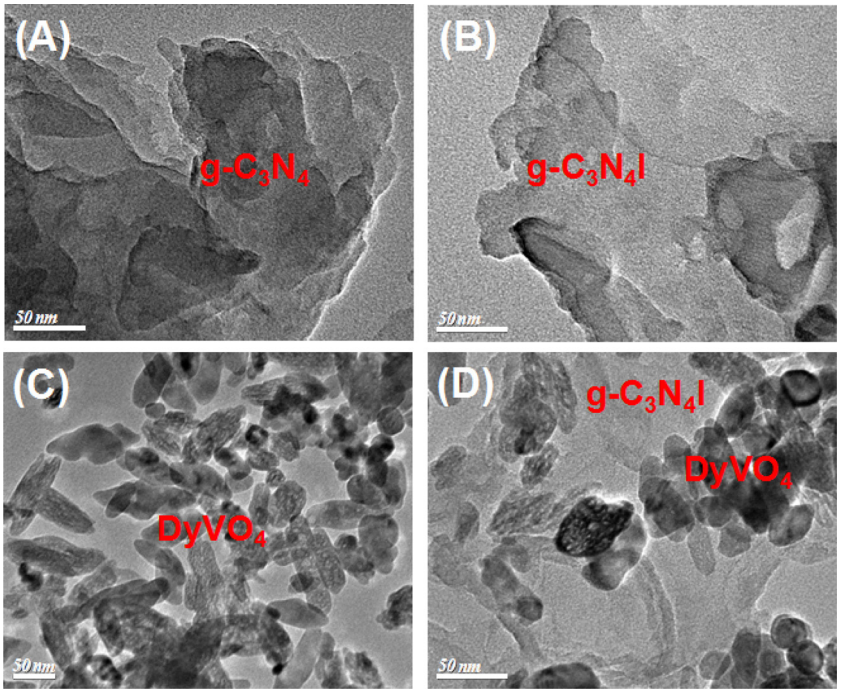

Fig. 4. TEM images of g-C_3N_4, g-C_3N_4I, $DyVO_4$ and 6.3% $DyVO_4$/g-C_3N_4I samples.

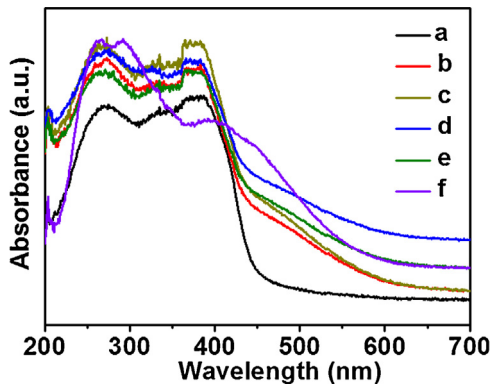

Fig. 5. UV–vis DRS of (a) g-C_3N_4, (b) g-C_3N_4I, (c) 3.2% $DyVO_4$/g-C_3N_4I, (d) 6.3% $DyVO_4$/g-C_3N_4I, (e) 9.7% $DyVO_4$/g-C_3N_4I, and (f) $DyVO_4$ samples.

The formation of the composite between g-C_3N_4I and $DyVO_4$ is demonstrated clearly by the TEM images (Fig. 4). A typical layered platelet-like surface morphology (Fig. 4A and B) and a rod-like nanostructure with an average particle size of approximately 25 nm (Fig. 4C) are identified for g-C_3N_4, g-C_3N_4I and $DyVO_4$, respectively [12,23]. In Fig. 4D, it can be seen that $DyVO_4$ is packed closely onto g-C_3N_4I, both of which are integrated together as an composite, and $DyVO_4$ is grafted on the surface of g-C_3N_4I, which results in the $DyVO_4$/g-C_3N_4I hybrid.

The UV–vis diffuse reflectance spectra of g-C_3N_4, g-C_3N_4I, 3.2% $DyVO_4$/g-C_3N_4I, 6.3% $DyVO_4$/g-C_3N_4I, 9.7% $DyVO_4$/g-C_3N_4I and $DyVO_4$ samples are shown in Fig. 5. It can be observed that there is a clear red-shift of the absorption of the g-C_3N_4I and $DyVO_4$/g-C_3N_4I composites in comparison with that of g-C_3N_4. All samples show absorption in the 400–700 nm visible-light region, and the photo-absorption ability of $DyVO_4$ is stronger than that of g-C_3N_4 and g-C_3N_4I. According to the previously reported strategy [12,14,23,26], the estimated optical absorption band gap for 3.2% $DyVO_4$/g-C_3N_4I, 6.3% $DyVO_4$/g-C_3N_4I, 9.7% $DyVO_4$/g-C_3N_4I and $DyVO_4$ semiconductors, is 2.65, 2.61, 2.64 and 2.32 eV, respectively, which is smaller than that of g-C_3N_4 (2.70 eV) and g-C_3N_4I (2.68 eV). Therefore, the interaction between g-C_3N_4I and $DyVO_4$ in the $DyVO_4$/g-C_3N_4I composite may contribute to the narrowing of the band gap due to the modified electronic structures. Interestingly, the content of $DyVO_4$ in the 9.7% $DyVO_4$/g-C_3N_4I sample is higher, but the band gap of 6.3% $DyVO_4$/g-C_3N_4I is 0.03 eV lower than that of 9.7% $DyVO_4$/g-C_3N_4I, suggesting the interaction between g-C_3N_4I and $DyVO_4$ can contribute to the best photoresponse and the narrowest band gap among the as-prepared $DyVO_4$/g-C_3N_4I samples.

Photoluminescence (PL) emission spectroscopy has been used as a tool to reveal the transfer and separation efficiency of photo-generated charge carriers [14,27,28]. The PL emission spectra of g-C_3N_4, g-C_3N_4I and 6.3% $DyVO_4$/g-C_3N_4I samples were measured at room temperature with an excitation wavelength of 400 nm (Fig. 6A). Obviously, a strong PL emission peak is observed for g-C_3N_4, which can be attributed to the radiative recombination of charge carriers [12,14]. Compared with g-C_3N_4 or g-C_3N_4I, the emission peak position of the 6.3% $DyVO_4$/g-C_3N_4I composite is hardly changed, but its relative intensity is lower, suggesting that the combination of $DyVO_4$ and g-C_3N_4I can significantly enhance the separation efficiency of the photo-induced electron–hole pairs.

Fig. 6B shows the EPR spectra of g-C_3N_4, g-C_3N_4I and 6.3% $DyVO_4$/g-C_3N_4I samples. A Lorentzian line centered at $g = 2.0034$ is observed, implying the generation of unpaired electrons on π-conjugated CN aromatic rings [14,29]. Clearly, this Lorentzian line is enhanced after the formation of the $DyVO_4$/g-C_3N_4I composite, presumably due to the redistribution of π electrons within the $DyVO_4$/g-C_3N_4I composite through band offsets [14]. Hence, the formation of $DyVO_4$/g-C_3N_4I composite is helpful for charge migration and separation by optimizing the electronic band structure.

Fig. 7A and B shows the electrochemical impedance spectroscopy and photocurrent tests of g-C_3N_4, g-C_3N_4I and 6.3% $DyVO_4$/g-C_3N_4I samples, respectively. An obvious decrease in the diameter of the Nyquist plot for 6.3% $DyVO_4$/g-C_3N_4I is observed (Fig. 7A), implying that the electronic resistance of 6.3% $DyVO_4$/g-C_3N_4I is smaller than that of g-C_3N_4 and g-C_3N_4I [12,14,30], which is also supported by the photocurrent tests (Fig. 7B). An improved photocurrent for 6.3% $DyVO_4$/g-C_3N_4I is generated, which is 3.6 and 1.2 times higher than that of g-C_3N_4 and g-C_3N_4I, respectively, indicating strongly that the separation and migration of the photo-excited charge carriers is improved in the 6.3% $DyVO_4$/g-C_3N_4I composite [14,31], which is consistent with the results of PL.

3.2. Photocatalytic property

The visible-light photocatalytic activity of the as-prepared g-C_3N_4, g-C_3N_4I, 3.2% $DyVO_4$/g-C_3N_4I, 6.3% $DyVO_4$/g-C_3N_4I, 9.7% $DyVO_4$/g-C_3N_4I and $DyVO_4$ samples was evaluated by the photodegradation of methylene blue (Fig. 8A), which is used commonly to test the degradation capability of catalysts. When methylene blue in an aqueous solution is irradiated with visible light for 4.0 h in the absence of a photocatalyst, little change in the methylene blue concentration is observed, which shows that the self-photodegradation of methylene blue is very limited. As the $DyVO_4$ content in the $DyVO_4$/g-C_3N_4I composites increases from 3.2% to 9.7%, the photocatalytic activity of the $DyVO_4$/g-C_3N_4I composites first increases and then decreases, and 6.3% $DyVO_4$/g-C_3N_4I indicates the highest activity. The photocatalytic activity of 6.3% $DyVO_4$/g-C_3N_4I is obviously higher than that of g-C_3N_4, g-C_3N_4I and $DyVO_4$. After 4.0 h irradiation, approximately 65% of methylene

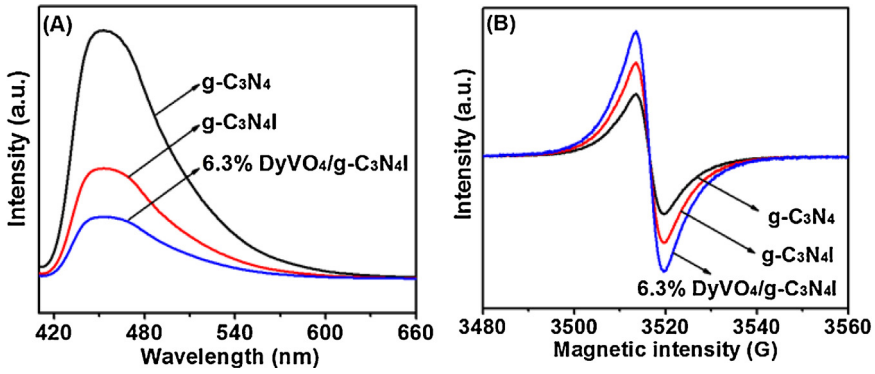

Fig. 6. (A) PL and (B) EPR spectra of g-C_3N_4, g-C_3N_4I and 6.3% $DyVO_4$/g-C_3N_4I samples.

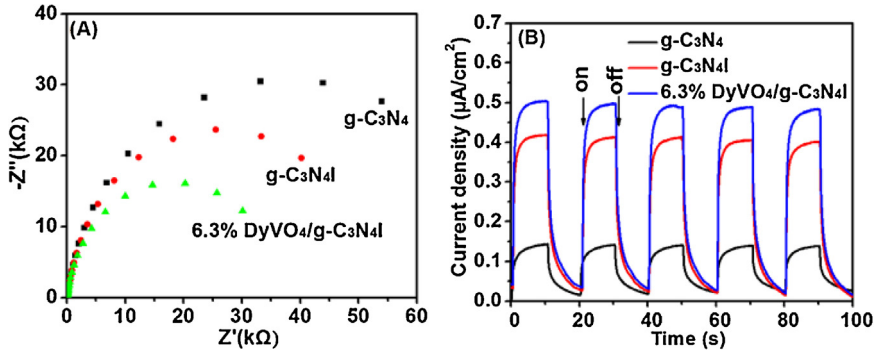

Fig. 7. (A) Electrochemical impedance spectroscopy and (B) transient photocurrents ($\lambda > 420$ nm) for g-C_3N_4, g-C_3N_4I and 6.3% $DyVO_4$/g-C_3N_4I samples.

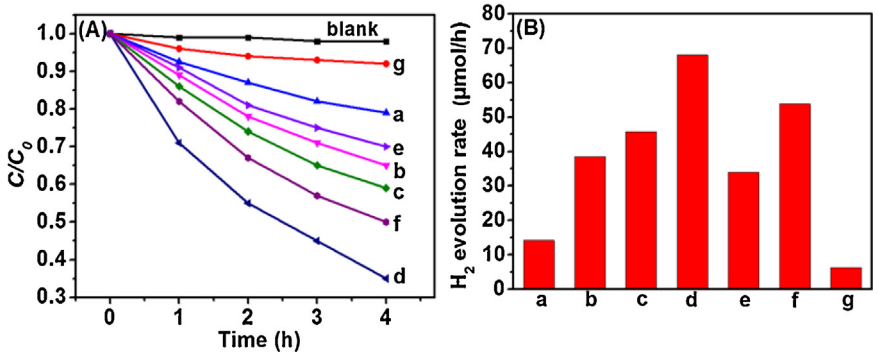

Fig. 8. (A) Photo-degradation of methylene blue and (B) photocatalytic hydrogen evolution rates for (a) g-C_3N_4, (b) g-C_3N_4I, (c) 3.2% $DyVO_4$/g-C_3N_4I, (d) 6.3% $DyVO_4$/g-C_3N_4I, (e) 6.3% $DyVO_4$/g-C_3N_4I (physical mixture), (f) 9.7% $DyVO_4$/g-C_3N_4I, and (g) $DyVO_4$ samples under visible-light irradiation ($\lambda > 420$ nm).

blue is removed by 6.3% $DyVO_4$/g-C_3N_4I, while only 21%, 35% and 8% of methylene blue degradation are achieved by g-C_3N_4, g-C_3N_4I and $DyVO_4$, respectively.

The photocatalytic H_2 production over g-C_3N_4, g-C_3N_4I, 3.2% $DyVO_4$/g-C_3N_4I, 6.3% $DyVO_4$/g-C_3N_4I, 9.7% $DyVO_4$/g-C_3N_4I and $DyVO_4$ photocatalysts was also studied (Fig. 8B). It can be observed that the photocatalytic efficiency for H_2 evolution exhibits a similar trend to that of methylene blue degradation with increasing $DyVO_4$ content in the $DyVO_4$/g-C_3N_4I composites. The photocatalytic H_2 evolution rate (68 μmol/h, with a quantum efficiency of ~1.8% at 405 nm) of 6.3% $DyVO_4$/g-C_3N_4I is 4.7, 1.7 and 10.6 times higher that that of g-C_3N_4, g-C_3N_4I and $DyVO_4$, respectively.

In order to underline the necessity of good interconnection between g-C_3N_4I and $DyVO_4$ for $DyVO_4$/g-C_3N_4I composites, 6.3% $DyVO_4$/g-C_3N_4I (physical mixture) was also tested for photocatalytic activity (Fig. 8). It can be seen that the photocatalytic activity of 6.3% $DyVO_4$/g-C_3N_4I (physical mixture) is obviously lower than that of 6.3% $DyVO_4$/g-C_3N_4I (Fig. 8A and B), elucidating the merit of hybridization.

3.3. Reactive species in the degradation of methylene blue

As been well known, superoxide radicals ($^{\bullet}O_2^-$), holes (h^+), hydroxyl radicals ($^{\bullet}OH$) and/or H_2O_2 are possibly reactive species for the photocatalytic degradation of organic pollutants [32–35]. In order to study which of these species are involved in methylene blue degradation, we used benzoquinone (BQ), ammonium oxalate (AO), isopropanol (IPA) and catalase (CAT) as $^{\bullet}O_2^-$, h^+, $^{\bullet}OH$ and H_2O_2 radical scavengers, respectively. By adding different scavengers to the photocatalytic reaction of methylene blue to remove the corresponding reactive species, the role of different reactive species in methylene blue photocatalytic process can be evaluated by the change of photocatalytic efficiency.

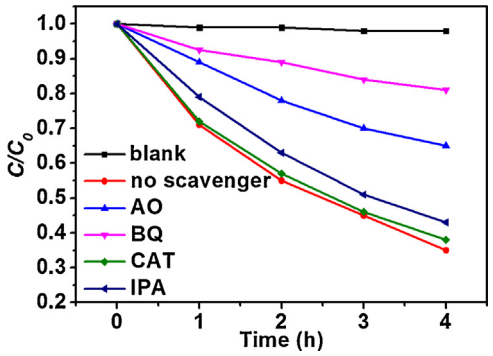

Fig. 9. Trapping test of photo-generated holes and radicals in the 6.3% $DyVO_4$/g-C_3N_4I photocatalytic system under visible-light irradiation ($\lambda > 420$ nm).

In Fig. 9, it can be seen that the addition of CAT or IPA causes a slight change in the photo-degradation efficiency of 6.3% $DyVO_4$/g-C_3N_4I. This shows that H_2O_2 or $^{\bullet}OH$ is not a significant active species in the photocatalytic process of methylene blue. However, an obvious suppression of photocatalytic activity is observed when BQ or AO is added, confirming the important role of $^{\bullet}O_2^-$ and h^+ in this system. Based on these results, it can be deduced that the photocatalytic degradation of methylene blue is mainly governed by $^{\bullet}O_2^-$ and h^+ rather than by H_2O_2 or $^{\bullet}OH$.

According to the above discussion, the probable reactions that occur in the photo-degradation of methylene blue are shown in Eqs. (1)–(4):

$$\text{Catalyst}(DyVO_4/g\text{-}C_3N_4I) + h\nu \rightarrow e^- + h^+ \quad (1)$$

$$e^- + O_2 \rightarrow {}^{\bullet}O_2^- \quad (2)$$

$$\text{methyleneblue} + h^+ \rightarrow \text{products} \quad (3)$$

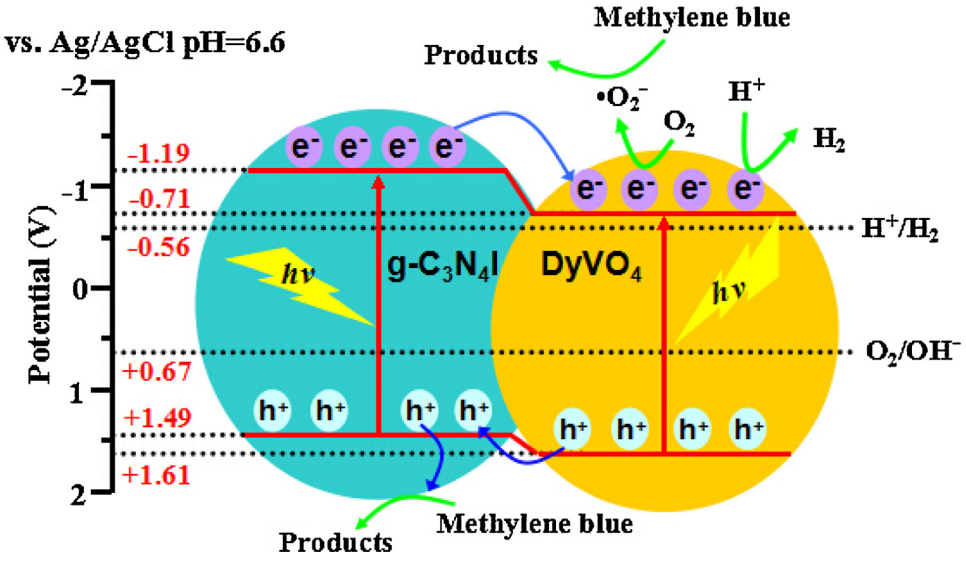

Fig. 10. Scheme for generation, transportation, and separation of visible-light-induced charge carries over the $DyVO_4$/g-C_3N_4I composite photocatalysts.

methyleneblue + $^{\bullet}O_2^-$ → products (4)

3.4. The mechanism of the enhanced photoactivity

According to the previously reported strategy [15,36–38], the bottom conduction band and top valence band potentials of $DyVO_4$ and g-C_3N_4I are calculated to be −0.71, +1.61, −1.19 and +1.49 V (vs. Ag/AgCl pH 6.6), respectively. As shown in Fig. 10, the conduction and valence band-edge between $DyVO_4$ and g-C_3N_4I are of very well matched positions. Once $DyVO_4$ and g-C_3N_4I are integrated together, the band alignment between the two semiconductors can drive the migration of photo-generated electrons (e^-) from g-C_3N_4I to $DyVO_4$ by the conduction band offset between g-C_3N_4I and $DyVO_4$, whereas the photo-induced holes (h^+) are transferred from $DyVO_4$ to g-C_3N_4I by the valence band offset [12,14,15,23]. The redistribution of electrons on one side of the junction ($DyVO_4$) and holes on the opposite side (g-C_3N_4I) can greatly reduce the recombination of electrons and holes, which was also confirmed by PL spectroscopy (Fig. 6A), electrochemical impedance spectroscopy (Fig. 7A) and photocurrent measurements (Fig. 7B). The successful separation of the photo-generated charge carriers in the $DyVO_4$/g-C_3N_4I composite, which can increase the lifetime of the charge carriers and enhance the efficiency of the interfacial charge transfer to adsorbed substrates [14,15], and then promote photoredox reactions. Therefore, the photoactivity of g-C_3N_4I is greatly enhanced after it is hybridized by $DyVO_4$.

This change of visible-light photoactivity for the $DyVO_4$/g-C_3N_4I composites may be attributed to two aspects. First, with the increase of $DyVO_4$ content in the $DyVO_4$/g-C_3N_4I composites from 3.2% to 6.3%, a greater contact area between $DyVO_4$ and g-C_3N_4I will be formed, which promotes the efficient separation of photo-induced electron–hole pairs, leading to the enhancement of the photoactivity. Second, if the content of $DyVO_4$ increases continuously to excess, excess $DyVO_4$ may decrease the quality of effective contacts between $DyVO_4$ and g-C_3N_4I, which is unfavorable for the transfer and separation of photo-generated charge carriers at the heterointerfaces. Moreover, excessive $DyVO_4$ coverage on the surface of g-C_3N_4I can block the active sites. Therefore, the photoactivity of the $DyVO_4$/g-C_3N_4I composites first increases and then decreases with the increasing $DyVO_4$ content, which results in the optimal photoactivity of 6.3% $DyVO_4$/g-C_3N_4I.

3.5. Stability test

It is widely known that the stability of the photocatalytic material is very important for its practical application. Therefore, the stability of $DyVO_4$/g-C_3N_4I composites during the photocatalytic reaction was studied by recycling tests, using 6.3% $DyVO_4$/g-C_3N_4I as a representative photocatalyst under the same condition (Fig. 11). It can be observed that there is no obvious change in the visible-light photocatalytic activity after four cycles, suggesting that 6.3% $DyVO_4$/g-C_3N_4I composite was not photocorroded during the photocatalytic process and retained good stability, which can be

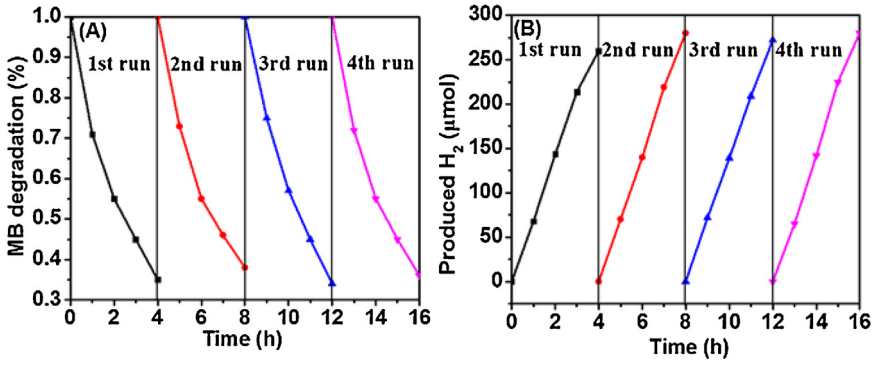

Fig. 11. Stability test of (A) methylene blue and (B) H_2 photosynthesis (evacuation every 4 h) for 6.3% $DyVO_4$/g-C_3N_4I under visible-light irradiation (λ > 420 nm).

attributed to the high separation and transfer of the photo-induced electron–hole pairs at the interfaces between $DyVO_4$ and g-C_3N_4I [14,39].

4. Conclusions

In summary, $DyVO_4$/g-C_3N_4I composite semiconductor photocatalysts were successfully fabricated by a facile calcination method at 550 °C. Compared with g-C_3N_4, g-C_3N_4I and $DyVO_4$, the $DyVO_4$/g-C_3N_4I composites showed a higher photo-degradation efficiency for methylene blue and a higher photocatalytic H_2 production rate under visible light irradiation. The 6.3% $DyVO_4$/g-C_3N_4I composite owned the highest photocatalytic activity for hydrogen evolution and the degradation of dye. The degradation ratio of methylene blue for the 6.3% $DyVO_4$/g-C_3N_4I sample was more than 1.8 time higher than that of g-C_3N_4, g-C_3N_4I and $DyVO_4$, whereas its H_2 evolution rate was 4.7, 1.7 and 10.6 times higher than that of g-C_3N_4, g-C_3N_4I and $DyVO_4$, respectively. There is no obvious change in photoactivity after four photocatalytic operation cycles. In the degradation of methylene blue, $^{\bullet}O_2^-$ and h^+ species played a major role and the role of $^{\bullet}OH$ and H_2O_2 species are negligible. This work not only highlights the photocatalytic degradation of methylene blue and H_2 generation for $DyVO_4$/g-C_3N_4I composites, but also provides relevant information for the future function-led design of multifunctional composite semiconductors applied in the field of energy and environment.

Acknowledgements

This work is financially supported by the National Basic Research Program of China (2013CB632405), the National Natural Science Foundation of China (21425309 and 21173043), the Natural Science Foundation of Higher Education Institutions in Anhui Province of China (KJ2014A191, 2015KJ011), Project Funded by China Postdoctoral Science Foundation (2015M571961), Postdoctoral Scientific Research Start-up Funding of Fuzhou University in China (601116), College Students' Innovative Training Program of China (AH201410371077), School-Level Item (FSB201401003, 2014KJFH01) of Fuyang Normal University of China, and Anhui Provincical Key Laboratory for Degradation and Monitoring of Pollution of the Environment in China.

References

[1] Y. Zheng, L.H. Lin, B. Wang, X.C. Wang, Angew. Chem. Int. Ed. 54 (2015) 12868–12884.
[2] K. Schwinghammer, M.B. Mesch, V. Duppel, C. Ziegler, J. Senker, B.V. Lotsch, J. Am. Chem. Soc. 136 (2014) 1730–1733.
[3] J.S. Zhang, M.W. Zhang, L.H. Lin, X.C. Wang, Angew. Chem. Int. Ed. 54 (2015) 6297–6301.
[4] S.-W. Cao, Y.P. Yuan, J. Barber, S.C.J. Loo, C. Xue, Appl. Surf. Sci. 319 (2014) 344–349.
[5] S.M. Wang, D.L. Li, C. Sun, S.G. Yang, Y. Guan, H. He, Appl. Catal. B: Environ. 144 (2014) 885–892.
[6] Y.Z. Hong, Y.H. Jiang, C.S. Li, W.Q. Fan, X. Yan, M. Yan, W.D. Shi, Appl. Catal. B: Environ. 180 (2016) 663–673.
[7] S.W. Cao, J.G. Yu, J. Phys. Chem. Lett. 5 (2014) 2101–2107.
[8] K. Srinivasu, B. Modak, S.K. Ghosh, J. Phys. Chem. C 118 (2014) 26479–26484.
[9] J.N. Qin, S.B. Wang, H. Ren, Y.D. Hou, X.C. Wang, Appl. Catal. B: Environ. 179 (2015) 1–8.
[10] Y. Ishida, L. Chabanne, M. Antonietti, M. Shalom, Langmuir 30 (2014) 447–451.
[11] Y.-P. Zhu, M. Li, Y.-L. Liu, T.-Z. Ren, Z.-Y. Yuan, J. Phys. Chem. C 118 (2014) 10963–10971.
[12] G.G. Zhang, M.W. Zhang, X.X. Ye, X.Q. Qiu, S. Lin, X.C. Wang, Adv. Mater. 26 (2014) 805–809.
[13] Q. Han, C.G. Hu, F. Zhao, Z.P. Zhang, N. Chen, L.T. Qu, J. Mater. Chem. A 3 (2015) 4612–4619.
[14] H.Q. Li, Y.X. Liu, X. Gao, C. Fu, X.C. Wang, ChemSusChem 8 (2015) 1189–1196.
[15] J.S. Zhang, M.W. Zhang, R.Q. Sun, X.C. Wang, Angew. Chem. Int. Ed. 51 (2012) 10145–10149.
[16] L. Ge, C.C. Han, J. Liu, Appl. Catal. B: Environ. 108–109 (2011) 100–107.
[17] S. Kumar, T. Surendar, A. Baruah, V. Shanker, J. Mater. Chem. A 1 (2013) 5333–5340.
[18] H.G. Kim, P.H. Borse, W.Y. Choi, J.S. Lee, Angew. Chem. 117 (2005) 4661–4665.
[19] Ch. Fettkenhauer, G. Clavel, K. Kailasam, M. Antonietti, D. Dontsova, Green Chem. 17 (2015) 3350–3361.
[20] S. Kumar, A. Baruah, S. Tonda, B. Kumar, V. Shanker, B. Sreedhar, Nanoscale 6 (2014) 4830–4842.
[21] Y.M. He, L.H. Zhao, Y.J. Wang, H.J. Lin, T.T. Li, X.T. Wu, Y. Wu, Chem. Eng. J. 169 (2011) 50–57.
[22] J.S. Zhang, X.F. Chen, K. Takanabe, K. Maeda, K. Domen, J.D. Epping, X.Z. Fu, M. Antonietti, X.C. Wang, Angew. Chem. Int. Ed. 49 (2010) 441–444.
[23] Y.M. He, J. Cai, T.T. Li, Y. Wu, Y.M. Yi, M.F. Luo, L.H. Zhao, Ind. Eng. Chem. Res. 51 (2012) 14729–14737.
[24] J.S. Zhang, M.W. Zhang, C. Yang, X.C. Wang, Adv. Mater. 26 (2014) 4121–4125.
[25] S. Zhou, Y. Liu, J.M. Li, Y.J. Wang, G.Y. Jiang, Z. Zhao, D.X. Wang, A.J. Duan, J. Liu, Y.C. Wei, Appl. Catal. B: Environ. 158–159 (2014) 20–29.
[26] J. Ding, L. Wang, Q.Q. Liu, Y.Y. Chai, X. Liu, W.-L. Dai, Appl. Catal. B: Environ. 176 (2015) 91–98.
[27] T. Kawahara, Y. Konishi, H. Tada, N. Tohge, J. Nishii, S. Ito, Angew. Chem. Int. Ed. 41 (2002) 2811–2813.
[28] V. Etacheri, M.K. Seery, S.J. Hinder, S.C. Pillai, Chem. Mater. 22 (2010) 3843–3853.
[29] J.S. Zhang, G.G. Zhang, X.F. Chen, S. Lin, L. Möhlmann, G. Dołęga, G. Lipner, M. Antonietti, S. Blechert, X.C. Wang, Angew. Chem. Int. Ed. 51 (2012) 3183–3187.
[30] Z.X. Pei, L.Y. Ding, M.L. Lu, Z.H. Fan, S.X. Weng, J. Hu, P. Liu, J. Phys. Chem. C 118 (2014) 9570–9577.
[31] Y. Pihosh, I. Turkevych, K. Mawatari, T. Asai, T. Hisatomi, J. Uemura, M. Tosa, K. Shimamura, J. Kubota, K. Domen, T. Kitamori, Small 10 (2014) 3692–3699.
[32] G.T. Li, K.H. Wong, X. Zhang, C. Hu, J.C. Yu, R.C. Chan, P.K. Wong, Chemosphere 76 (2009) 1185–1191.
[33] L.S. Zhang, K.H. Wong, H.Y. Yip, C. Hu, J.C. Yu, C.Y. Chan, P.K. Wong, Environ. Sci. Technol. 44 (2010) 1392–1398.
[34] M.C. Yin, Z.S. Li, J.H. Kou, Z.G. Zou, Environ. Sci. Technol. 43 (2009) 8361–8366.
[35] J.S. Zhang, Y. Chen, X.C. Wang, Energy Environ. Sci. 8 (2015) 3092–3108.
[36] L.K. Randeniya, A. Bendavid, P.J. Martin, E.W. Preston, J. Phys. Chem. C 111 (2007) 18334–18340.
[37] A.I. Kontos, V. Likodimos, T. Stergiopoulos, D.S. Tsoukleris, P. Falaras, Chem. Mater. 21 (2009) 662–672.
[38] X. Wang, Q. Xu, M.R. Li, S. Shen, X.L. Wang, Y.C. Wang, Z.C. Feng, J.Y. Shi, H.X. Han, C. Li, Angew. Chem. Int. Ed. 51 (2012) 1–5.
[39] J. Fu, B.B. Chang, Y.L. Tian, F.N. Xi, X.P. Dong, J. Mater. Chem. A 1 (2013) 3083–3090.